Engineering 22 (2023) 201–214

Contents lists available at ScienceDirect

Engineering

journal homepage: www.elsevier.com/locate/eng

Research
Climate Change—Article

Long-Term Observations of Atmospheric Constituents at the First Ground-Based High-Resolution Fourier-Transform Spectrometry Observation Station in China

Cheng Liu [a,b,c,d,e], Youwen Sun [a,b,*], Changgong Shan [b], Wei Wang [b], Justus Notholt [f], Mathias Palm [f], Hao Yin [a,c], Yuan Tian [g], Jixi Gao [h], Huiqin Mao [h]

[a] Department of Precision Machinery and Precision Instrumentation, University of Science and Technology of China, Hefei 230026, China
[b] Key Laboratory of Environmental Optics and Technology, Anhui Institute of Optics and Fine Mechanics, Hefei Institutes of Physical Science, Chinese Academy of Sciences, Hefei 230031, China
[c] Center for Excellence in Regional Atmospheric Environment, Institute of Urban Environment, Chinese Academy of Sciences, Xiamen 361021, China
[d] Key Laboratory of Precision Scientific Instrumentation of the Anhui Higher Education Institutes, University of Science and Technology of China, Hefei 230026, China
[e] Anhui Province Key Laboratory of the Polar Environment and Global Change, University of Science and Technology of China, Hefei 230026, China
[f] Institute of Environmental Physics, University of Bremen, Bremen 28334, Germany
[g] Institutes of Physical Science and Information Technology, Anhui University, Hefei 230601, China
[h] Satellite Application Center for Ecology and Environment, Ministry of Ecology and Environment of the People's Republic of China, Beijing 100094, China

ARTICLE INFO

Article history:
Received 3 June 2021
Revised 6 October 2021
Accepted 15 November 2021
Available online 17 February 2022

Keywords:
Remote sensing
Fourier-transform
Atmospheric pollution
Greenhouse gases
Climate change

ABSTRACT

Long-term observations of the volume mixing ratio (VMR) profiles and total columns of key atmospheric constituents are significant for understanding climate change and the impact of the carbon budget in China. This study provides an overview of the first ground-based high-resolution Fourier-transform spectrometry (FTS) observation station in China, which is located in Hefei, east China. The FTS observation station can observe the total columns and VMR profiles of more than 30 atmospheric constituents. Time series of some key atmospheric constituents observed at the Hefei station since 2014 have been released to the public. The major scientific achievements obtained to date at this station include spectral retrieval characterization and harmonization, investigation of the overall characteristics of key atmospheric constituents, emission estimates, satellite and chemical transport model (CTM) evaluations, and a summary of pollutant sources and transport patterns. An outlook is also presented of the envisaged plan for observations, scientific studies, and data usage at the Hefei station. China has explicitly proposed reaching a peak in its CO_2 emissions by 2030 and realizing carbon neutrality by 2060. The Hefei station will provide scientific assistance to the Chinese Government for developing green economy policies and achieving carbon neutrality and the goals of the Paris Agreement.

© 2022 THE AUTHORS. Published by Elsevier LTD on behalf of Chinese Academy of Engineering and Higher Education Press Limited Company. This is an open access article under the CC BY-NC-ND license (http://creativecommons.org/licenses/by-nc-nd/4.0/).

1. Introduction

Air pollution has been one of China's greatest challenges in recent decades [1,2]. In particular, megacity clusters in east China have endured heavy air pollution due to intensive anthropogenic activities [3–9]. In recent years, however, air pollution across China has dramatically decreased due to a series of measures taken to reduce emissions [10,11]. Nevertheless, the atmospheric pollution over highly industrialized and densely populated east China is still severe [12,13]. The severity, expanse, and complexity of the atmospheric pollution in this region remain unrivaled in comparison with the rest of the world [11,13–15]. Long-term observations of the volume mixing ratio (VMR) profiles and total columns of key atmospheric constituents are necessary to understand the sources, chemical mechanisms, and transport processes of air pollution and carbon emissions in China, as well as for potential regulatory and control purposes [15]. In addition, precise detection of the burdens and variabilities of key tropospheric (e.g., CO, CO_2, CH_4, N_2O, C_2H_6, SF_6, carbonyl sulfide (OCS), H_2CO, HCN, and peroxyacetyl nitrate (PAN)) and stratospheric (e.g., O_3, HNO_3, HF, HCl, and $ClONO_2$)

* Corresponding author.
E-mail address: ywsun@aiofm.ac.cn (Y. Sun).

https://doi.org/10.1016/j.eng.2021.11.022
2095-8099/© 2022 THE AUTHORS. Published by Elsevier LTD on behalf of Chinese Academy of Engineering and Higher Education Press Limited Company.
This is an open access article under the CC BY-NC-ND license (http://creativecommons.org/licenses/by-nc-nd/4.0/).

species and an understanding of their influence on climate change are important for establishing scientific links between climate change and atmospheric constituents; validating satellite, airborne, or other ground-based observations; supporting process-focused field campaigns; and improving theoretical chemical transport models (CTMs) [16–19].

Ground-based high-resolution direct solar Fourier-transform spectrometry (FTS) has been established as a powerful tool to derive VMR profiles and total columns of atmospheric constituents [16,17,20–23]. Both the Total Carbon Column Observing Network (TCCON) and the Network for Detection of Atmospheric Composition Change (NDACC) utilize high-resolution FTS spectrometers to observe the variabilities of atmospheric constituents. The TCCON and NDACC networks have been operating since 2004 and 1992, respectively, and provide time series of total columns and VMR profiles of more than 30 atmospheric constituents. These results have been widely used in scientific investigations of the carbon cycle [24–30], atmospheric pollution and transport [8,10,13,31–34], and stratospheric ozone (O_3) [18]; the development of spectroscopic line lists and models [35–45]; the validation of satellite observations and satellite retrieval algorithm development [46–56]; and the evaluation of atmospheric CTMs [57–61]. However, most TCCON/NDACC stations are operated in North America and Europe, while operational stations in the rest of the world remain sparse. For now, there is only one qualified operational site within China: Hefei station (117.2°E, 32.0°N, 30.0 m above sea level (a.s.l.)) [8,15].

In this study, we provide an overview of the first ground-based high-resolution FTS observation station in China. The site is close to the Yangtze River Delta (YRD) in east China—one of the most highly industrialized and densely populated regions in the country, with complex pollution and carbon emission sources. We introduce the overall envisaged concept of the observation station, describe the site and instrumentation, and summarize the major achievements that have been made at this station, which include spectral retrieval characterization and harmonization, investigation of the overall characteristics of key atmospheric constituents, emission estimates, satellite and CTM evaluations, and results on the sources and transport patterns of the studied atmospheric constituents. An outlook of the envisaged plan for observations, scientific studies, and data usage at the Hefei station is also presented.

2. Site description and instrumentation

2.1. Envisaged concept and site description

The FTS station is located on Science Island in the suburbs of Hefei in highly industrialized and densely populated east China [62,63]. The Hefei station has run TCCON observations since July 2014 and became a formal TCCON station in 2018[†]. This station is not yet affiliated with the NDACC network, but its observation routine has followed the NDACC standard conventions since 2015 [8,17]. The FTS observatory is a cross-disciplinary observation platform developed by the Anhui Institute of Optics and Fine Mechanics, Chinese Academy of Sciences (AIOFM-CAS), in collaboration with the University of Science and Technology of China (USTC), and other TCCON/NDACC partners such as the University of Wollongong, Australia, and the University of Bremen, Germany. The observatory is part of the Atmospheric Environmental Observation and Simulation (AEOS) infrastructure, which is a National Mega-Project of Science Research of China; it includes many kinds of environmental instruments, simulators, and platforms for intensive atmospheric science research.

[†] https://tccondata.org/.

Hefei is populated by 7 million people, and the city center is located to the southeast of the station. In the other directions, the observation station is surrounded by cultivated lands or wetlands. The regional landscape around the station is mostly flat, with a few hills. The observatory is the only qualified station in China that has been performing long-term FTS observations of key atmospheric constituents; thus, it plays a crucial role in evaluating satellite observations, CTM simulations, air quality, and the long-range transport of atmospheric pollutants arising from anthropogenic and natural emissions in this important region [63].

Benefiting from its unique geographical location, the Hefei station is an ideal site for investigating the physical processes of air masses from different origins and the atmospheric chemistry interactions along the transport paths. Hefei is the starting point of a series of city clusters along the Hefei-to-Shanghai axis in the YRD region. It is generally downwind of the regional anthropogenic and natural sources under the southeasterly wind in summer and northeasterly wind in winter. As a result, its location is ideal for investigating the physical and chemical processes of atmospheric constituents after sufficient mixing and chemical reactions [64]. Hefei is also located at the southern tip of the North China Plain, which contains another highly industrialized and densely populated region in China: the Beijing–Tianjin–Hebei (BTH) region. The northerly winter monsoon carries regional plumes from intensive fossil fuel and biomass burning (BB) sources in the BTH region to the Hefei station [13]. Furthermore, due to the influence of the summer monsoon in the warm season, the Hefei station is basically downwind of the tropical forest region in Southeast Asia (SEAS) and the subtropical forest region in southwest China, which have strong biogenic emissions. However, from a sub-synoptic perspective, the air masses arriving at Hefei in all seasons are influenced by cyclones or anti-cyclones originating from different regions [15,64].

2.2. Instrumentation

The observatory includes a high-resolution FTS spectrometer (IFS125HR, Bruker, Germany), a solar tracker, and a meteorological station (Fig. 1) [62,63]. The spectrometer is inside a room, whereas the solar tracker and weather station are installed directly on the building roof. Two air conditioners, a dehumidifier, and an air cleaner are operated uninterruptedly to obtain a constant temperature with dry and clean indoor conditions [62,63]. IFS125HR spectrometers exhibit outstanding capabilities in precision and stability during normal operations and have been widely used within the TCCON/NDACC networks [22,65]. The IFS125HR spectrometer at the Hefei station has six detectors, four beam splitters, and a maximum optical path difference (OPD) of 937.5 cm, corresponding to a maximum possible resolution of 0.001 cm^{-1}. All detector and beam splitter types, along with their work ranges, are summarized in Tables S1 and S2 in Appendix A, respectively. The spectrometer covers a wide spectral range from 420 to 50 000 cm^{-1}. The solar tracker is mounted inside a dome that consists of two spherical covers, which protects the solar tracker from bad weather such as rain, snow, and high wind speed. The rotation of the dome and the on/off state of the two spherical covers are controlled by three specific motors. The solar tracker tracks the Sun by adjusting two aluminized folding mirrors and guides the sunlight into the FTS spectrometer. Thanks to its Camtracker mode, the solar tracker can track the Sun with a precision of ±0.1 mrad [1] (1 rad = 57.3°). The meteorological station mounted near the dome includes sensors for air temperature (±0.30 °C), relative humidity (±3.0%), air pressure (±0.1 hPa), wind speed (±0.50 $m{\cdot}s^{-1}$), wind direction (±5.0°), solar radiation (±5.0% during daylight), and the presence of rain. These meteorological parameters are used to improve the spectral retrievals. The IFS125HR instrument is equipped with a

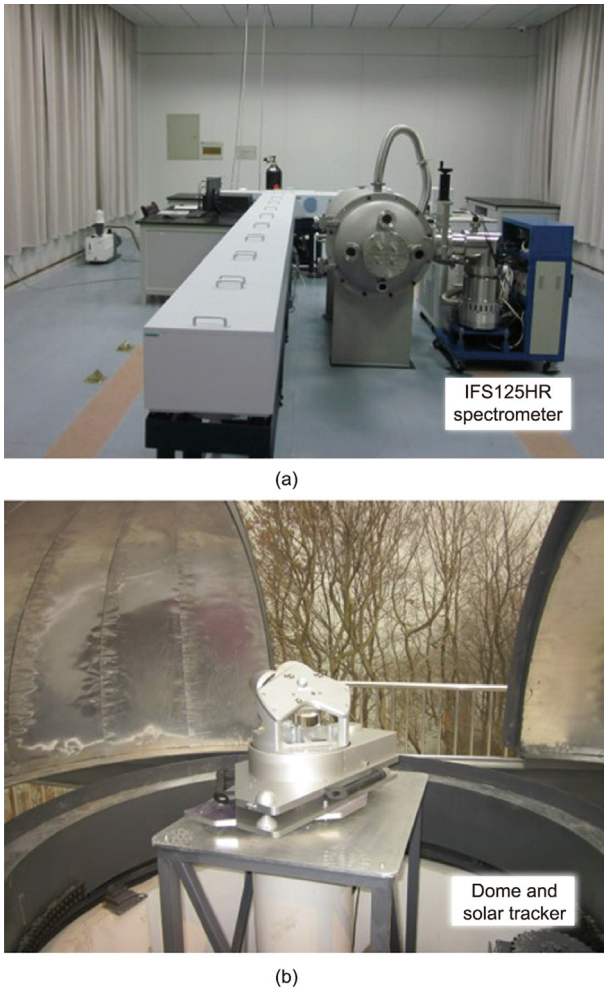

Fig. 1. The main components of the high-resolution FTS observatory at Hefei, China. (a) An IFS125HR spectrometer; (b) a dome and a solar tracker [62,63].

multi-stage scroll pump to keep the interferometer under a vacuum, which enhances the stability of the instrument and minimizes the absorption interference of water vapor.

We have operated the FTS observatory almost continuously since 2014. Before July 2015, we operated the FTS instrument to follow TCCON requirements and only collected near-infrared (NIR) solar spectra. We then modified the FTS instrument to collect NDACC observations in the middle-infrared (MIR) spectral range as well. Thereafter, NIR and MIR solar spectra were alternately collected in routine observations following the order shown in Table S3 in Appendix A. NIR and MIR spectra are collected with spectral ranges of 4000–11 000 cm^{-1} and 500–8500 cm^{-1}, temporal resolutions of 150 and 288 s, and spectral resolutions of 0.020 and 0.005 cm^{-1}, respectively. Both spectral resolutions can resolve the atmospheric absorption structures of all gases. Depending on the weather conditions, the number of both NIR and MIR spectra on each observation day vary from 11 to 103. An InGaAs detector and CaF_2 beam splitter are used for NIR spectra acquisition, but no filters are needed. For MIR spectra acquisition, an InSb or cadmium telluride mercury (MCT) detector, KBr beam splitter, and seven filters with different transmission wavenumbers are used. NIR spectra are used to retrieve the total columns of CO_2, CH_4, N_2O, HF, CO, H_2O, HCl, and HDO [17,62], while MIR spectra are used to retrieve VMR profiles and the total columns of O_3, CO_2, NO_2, N_2, NO, HNO_3, CO, HCl, HF, N_2O, CH_4, C_2H_6, HCN, $ClONO_2$, H_2O, HDO, ClO, OCS, H_2CO, C_2H_2, C_2H_4, CF_4, SF_6, CH_3D, COF_2, CCl_3F, CCl_2F_2, $CHClF_2$, C_3H_8, HCOOH, CH_3OH, PAN, and NH_3 [18,66]. The major research relevance and significance of these gases are summarized in Table 1, including validation, global warming, ozone chemistry, and regional pollution.

Table 1
Major research relevance and significance of the atmospheric constituents observed at the Hefei station.

Focus area	Significance/effect	Key atmospheric constituents
Validation	Satellite or CTM	CO_2, CH_4, N_2O, HF, CO, H_2O, HCl, HDO, O_3, NO_2, HNO_3, HCl, NO, C_2H_6, HCN, $ClONO_2$, H_2CO, C_2H_2, C_2H_4, SF_6, CCl_3F, CCl_2F_2, $CHClF_2$, HCOOH, CH_3OH, and NH_3
Global warming (radiative forcing)	Climate/environmental change	H_2O, HDO, CO_2, CH_4, CH_3D, N_2O, SF_6, O_3, C_2H_6, CCl_3F, CCl_2F_2, and $CHClF_2$
Ozone chemistry	Biological effects of ultraviolet–visible (UV–vis) exposure	O_3, ClO, HCl, $ClONO_2$, COF_2, NO, NO_2, and HNO_3
Regional pollution	Human health	CO, C_3H_8, HCN, H_2CO, COF_2, and O_3
	Photochemical smog	NO, HNO_3, NO_2, O_3, C_2H_2, H_2CO, C_2H_4, C_2H_6, PAN, and CO
	Acid rain	SO_2, NH_3, NO, HNO_3, and NO_2
	Oxidation efficiency of the atmosphere	HCOOH, CH_3OH, CO, H_2CO, CH_4, NO, NO_2, and O_3
	Source of aerosols and precursors	SO_2, HNO_3, CF_4, NH_3, and OCS (for stratospheric aerosols)

3. Methodology and characterization

3.1. Retrieval and characterization of the NIR spectra suite

We use the TCCON standard analysis software GGG to retrieve the total columns of atmospheric gases from the NIR solar spectra [17]. The GGG software was recently updated to version 2020, which has improved the *a priori* profiles for primary gases. Although GGG2020 will be used at the Hefei station in the near future, the NIR solar spectra that are reported in the present work were processed with the well-established GGG2014. The first step in GGG is to process the raw interferograms, correct them for phase errors and solar intensity variations, and convert them into spectra. The *a priori* profiles of meteorological parameters and trace gases are then generated, with the temperature, humidity, and pressure being based on analyses by the National Centers for Environmental Protection and the National Center for Atmospheric Research (NCEP/NCAR), and with the profiles of CO_2, CO, CH_4, and N_2O being based on the Mark IV Balloon Interferometer (MkIV) balloon flights, satellite atmospheric chemistry experiment-FTS (ACE-FTS), and GLOBALVIEW data. A series of influences such as the seasonal cycle, a secular increase, interhemispheric gradient, and stratospheric decay are considered. GGG then scales the *a priori* profiles iteratively to generate modeled spectra until an optimal fit to the measured spectra is achieved. Finally, the scaled profiles are integrated to compute the total column and are further converted into column-averaged dry air mole fractions (DMFs; referred to as X_G for gas G), with the total column of oxygen (O_2) being retrieved from the same spectra. This conversion process reduces the influence associated with surface pressure and H_2O variations, and improves the precision. Setups for retrieving all gases with the NIR spectra suite are summarized in Table S4 in Appendix A.

We follow the TCCON convention and use the formalism of Wunch et al. [22] to calculate the retrieval error. We conduct a series of sensitivity studies and perturb every source of error in the GGG forward model by a realistic range. We then calculate the fractional difference for each error source relative to the

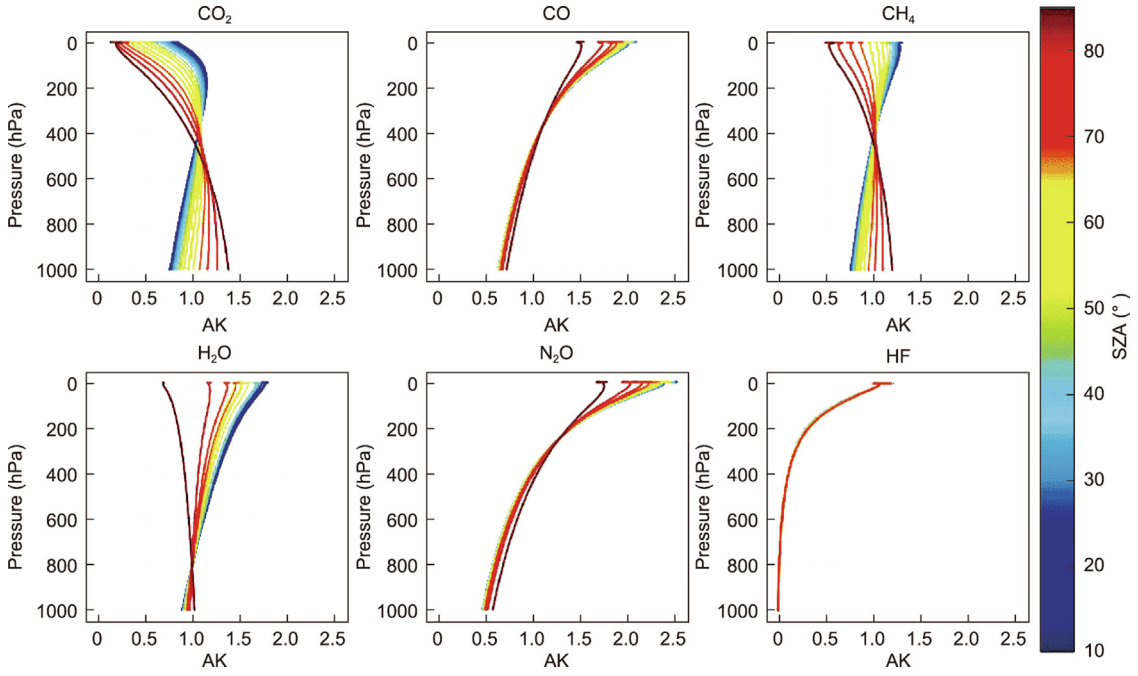

Fig. 2. TAKs of typical gases retrieved with the NIR spectra suite at the Hefei station AK: averaging kernel.

unperturbed case [17,62,63,67]. These sensitivities are calculated for spectra from a clear-sky day, over a large range of surface temperatures, solar zenith angles (SZAs), and water vapor amounts. In the sensitivity study, *a priori* profiles of X_{H_2O} and X_{HDO} are modified by reducing the surface concentrations by 50%. Other gases are modified by shifting the profiles down by 1 km in altitude. The *a priori* profiles of temperature and pressure are increased by 1 K and 1 hPa at all altitudes, respectively. The continuum curvature is modified by fitting a third-order continuum curvature to all windows wider than 20 cm^{-1}. Zero level offsets, pointing offsets, surface pressure, field of view (FOV), and observer–Sun Doppler stretch (OSDS) are increased by 0.1%, 0.05°, 1 hPa, 7%, and 2 parts per million by volume (ppmv), respectively. The alignment of the instrument is perturbed by ±5% of the ideal condition. The total error is calculated in quadrature for each individual error. The results show that the largest contributors to the uncertainty budget for all gases are shear misalignments, OSDS, *a priori* profile shape errors, *a priori* temperature profile errors, continuum curvature, and zero-level offsets. For SZAs less than 80°, the total errors of X_{CO_2}, X_{CH_4}, X_{N_2O}, X_{CO}, X_{H_2O}, X_{HDO}, and X_{HF} are less than 0.25% (~1 parts per million (ppm)), 0.50% (~5 parts per billion (ppb)), 1.00% (~3 ppb), 4.00% (~10 ppb), 1.30%, 2.00%, and 8.00% (~4 ppb), respectively.

Total column averaging kernels (TAKs) describe the height-dependent sensitivity in the retrieval to errors in the profile shape. For an ideal column observation, the TAKs should be 1.0 at all heights; in reality, however, greater or lesser sensitivities to some heights in comparison with others also exist. The TAKs at all TCCON stations are similar and are a function of the fitted parameters and the GGG profile scaling algorithm. The TAKs are also slightly dependent on the SZA during the measurement time. Fig. 2 shows the TAKs for the Hefei station. Since the pressure broadening of the spectroscopic lines in the stratosphere is narrower than that in the troposphere, gases with saturated atmospheric absorption lines are insensitive to variations in the stratosphere. As a result, the stratospheric TAKs decrease as the air mass increases.

Time series of X_{CO_2}, X_{CH_4}, X_{N_2O}, X_{CO}, X_{H_2O}, X_{HDO}, X_{HCl}, and X_{HF} retrieved with the NIR spectra suite at the Hefei station are shown in Fig. 3. As a formal TCCON station, all these datasets are archived in the TCCON database[†] under open access. The main achievements with these datasets are summarized in Section 4.

3.2. Retrieval and characterization of the MIR spectra suite

We use the latest NDACC standard analysis software SFIT4 (version 0.9.4.4) with an optimal estimation (OE) technique to process the MIR spectra suite [16,68]. As listed in Table S3, the MIR spectra suite at the Hefei station is capable of retrieving the total columns and VMR profiles of more than 30 atmospheric constituents, including ten NDACC-mandatory species—namely, CH_4, N_2O, CO, HCN, C_2H_6, O_3, $ClONO_2$, HNO_3, HF, and HCl—and many research-oriented species. Thus far, we have retrieved, analyzed, and investigated all the NDACC species and four research-oriented species: H_2CO, NO_2, CO_2, and SF_6. The retrieval settings for all NDACC gases follow the NDACC recommendations, as tabulated in Table S5 in Appendix A. For gases outside of the NDACC network, the retrieval settings are based on recommendations in Refs. [69–71]. The *a priori* profiles of all gases except water vapor (H_2O) are from the statistical averages of the Whole Atmosphere Community Climate Model (WACCM) v6 simulations from 1980 to 2020 [8]. The *a priori* profiles of pressure, temperature, and H_2O are extracted from the NCEP/NCAR 6 h reanalysis data. Depending on the gas, the spectroscopic parameters are provided by the HITRAN 2008 or HITRAN 2012 databases [8,10,67,71]. We deal with the absorption interference of H_2O differently for different gases. For all gases except $ClONO_2$ and HNO_3, the H_2O profile is retrieved together with the profile of the target gas. For $ClONO_2$ and HNO_3, we treat H_2O as another interfering species—that is, we only scale the *a priori* profile of H_2O. Since the abundance and interference are gas dependent, different de-weighting schemes are used for different gases. We use a de-weighting signal-to-noise ratio (SNR) of 500 for CO and 300 for HCl retrievals, but no de-weighting SNRs are used for other gases [72,73]. The empirical usage of these de-weighting SNRs can reduce

[†] https://tccondata.org/.

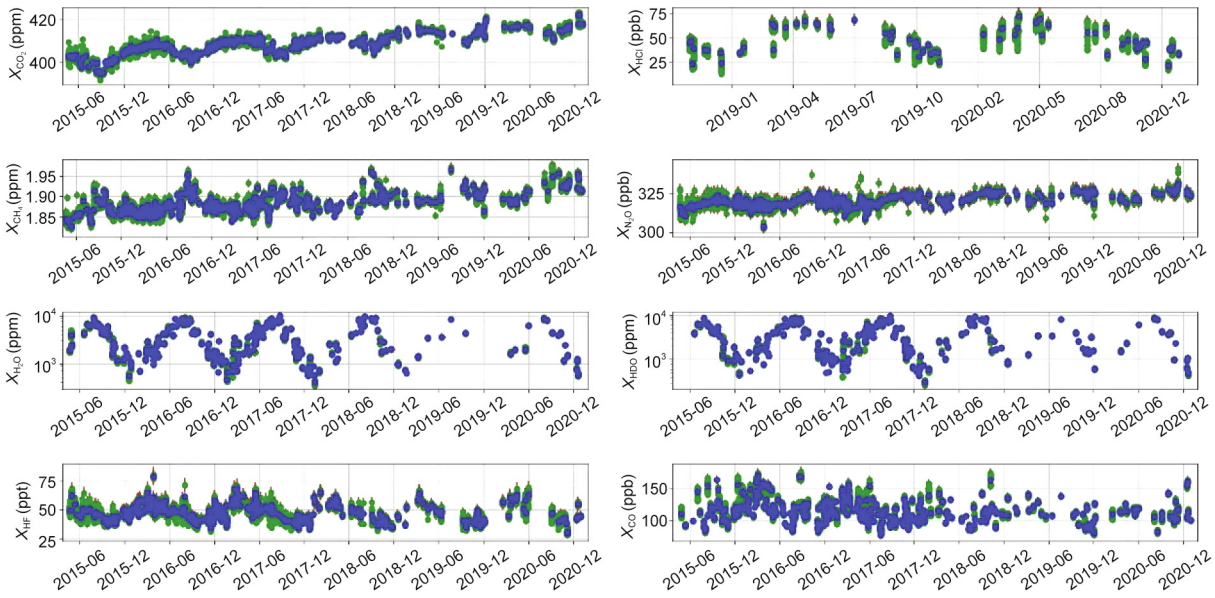

Fig. 3. Time series of the DMFs of typical gases retrieved with the NIR spectra suite at the Hefei station. Green and blue dots represent individual and daily mean results, while vertical error bars represent retrieval uncertainties ppt: parts per trillion.

the retrieval residual and improve the accuracy of the spectral retrieval for each gas. The diagonal values of the *a priori* covariance matrices $\boldsymbol{S}_a$ are set to the standard deviation of the WACCM v6 simulations. The abundances of some gases (e.g., CO_2, CH_4, and N_2O) have changed significantly since 1980, so the standard deviation of the WACCM simulations may overestimate the natural variabilities of these gases. In order to minimize the influence, Gaussian or exponential inter-layer correlation shapes are used for these gases to constrain the shapes of the retrieved profiles. The diagonal values of the noise covariance matrices $\boldsymbol{S}_\varepsilon$ are set to the inverse square of the spectral SNR. The non-diagonal values of $\boldsymbol{S}_a$ and $\boldsymbol{S}_\varepsilon$ are set to zero. The instrument line shape (ILS) available from optical alignment diagnosis is adopted in the retrieval [72,73].

For each retrieval, the averaging kernels (AKs) describe the height-dependent sensitivity. The area of the AKs at a selected height is calculated by summing up all the elements of the corresponding AKs [74]. This represents the fraction of the retrieval at that height, which comes from the measurement [68]. A value close to zero indicates that the retrieval is nearly independent of the measurement but is determined by the *a priori* information. The degrees of freedom for the signal (DOFS) are calculated as the trace of the AKs matrix and quantify the number of independent partial columns in the retrieval. The AKs and their areas for some MIR gases at the Hefei station are shown in Fig. 4. High-sensitivity ranges (i.e., a height range with a sensitivity of more than 0.5) for HCN, H_2CO, SF_6, CO, and C_2H_6 are in the troposphere; for HF, NO_2, and HCl, these are in the stratosphere, while for O_3 and CH_4, they are in both the stratosphere and troposphere. The typical DOFS over the total atmosphere for CH_4, NO_2, CO, HCN, C_2H_6, O_3, H_2CO, SF_6, HF, and HCl are 3.5, 1.0, 3.0, 1.1, 1.5, 4.8, 1.1, 1.0, 1.3, and 1.5, respectively. The potential independent altitude information to be retrieved from the measurements for CH_4, O_3, and CO at Hefei can be separated into three, four, and three independent partial layers, respectively. However, we can roughly obtain one degree of freedom on the profiles of HCl, NO_2, H_2CO, HF, SF_6, C_2H_6, and HCN.

The error budget for MIR spectra retrievals at Hefei is calculated using the formalism of Rodgers [68], and all error components are separated into random and systematic errors, as listed in Table S5. The covariance matrix of each interfering gas is prescribed from the WACCM v6 climatology. The covariance matrix of temperature is set to 3–7 K in the stratosphere and 2–5 K in the troposphere, based on the differences between the sonde and the NCEP temperature profiles. The covariance matrix of the measurement error is set to the inverse square of the spectral SNR. We regularly diagnose the optical alignment of the instrument and realign the interferometer when indicated. The FTS instrument at Hefei is assumed to be close to the ideal state, and the uncertainties for the FOV, OPD, interferogram phase, zero level, and background curvature are all assumed to be 1%. The covariance matrix for the retrieval parameter and smoothing error are prescribed from the SFIT4 retrieval outputs. Depending on the gas, we use 5% or 10% for uncertainties of line intensity, air-broadening, and self-broadening coefficients. Total retrieval error is calculated in quadrature for all systematic and random errors. Typical retrieval errors over the total atmosphere at the Hefei station for CH_4, NO_2, CO, HCN, C_2H_6, O_3, SF_6, H_2CO, HF, and HCl are estimated to be 4.5%, 12.4%, 4.7%, 11.3%, 6.2%, 5.7%, 5.8%, 12.3%, 5.1%, and 5.2%, respectively.

The total column time series of some typical gases retrieved with the MIR spectra suite at the Hefei station are shown in Fig. 5. Pronounced day-to-day variabilities and seasonality of these gases are observed. The main achievements that were made with the results retrieved from the MIR spectra suite are summarized in Section 4.

4. Main achievements obtained at the Hefei station

The Hefei station has archived almost seven years of high-quality data for many atmospheric constituents. We have conducted a series of studies with these datasets to understand high-resolution spectral retrieval and harmonization, investigate the overall characteristics of key atmospheric constituents, perform emission estimates and satellite and CTM evaluations, and determine seasonal levels of air pollution, along with its sources, transport, and chemical mechanisms. Table 2 [8,10,13,15,62,63,66,67,71,73,75–81] provides a summarized inventory of these studies based on FTS observations at the Hefei station during 2014–2020, categorized by key findings, data period, theme (i.e., the main gases considered), waveband, atmospheric domain, and topic. The main achievements at the Hefei station are as follows.

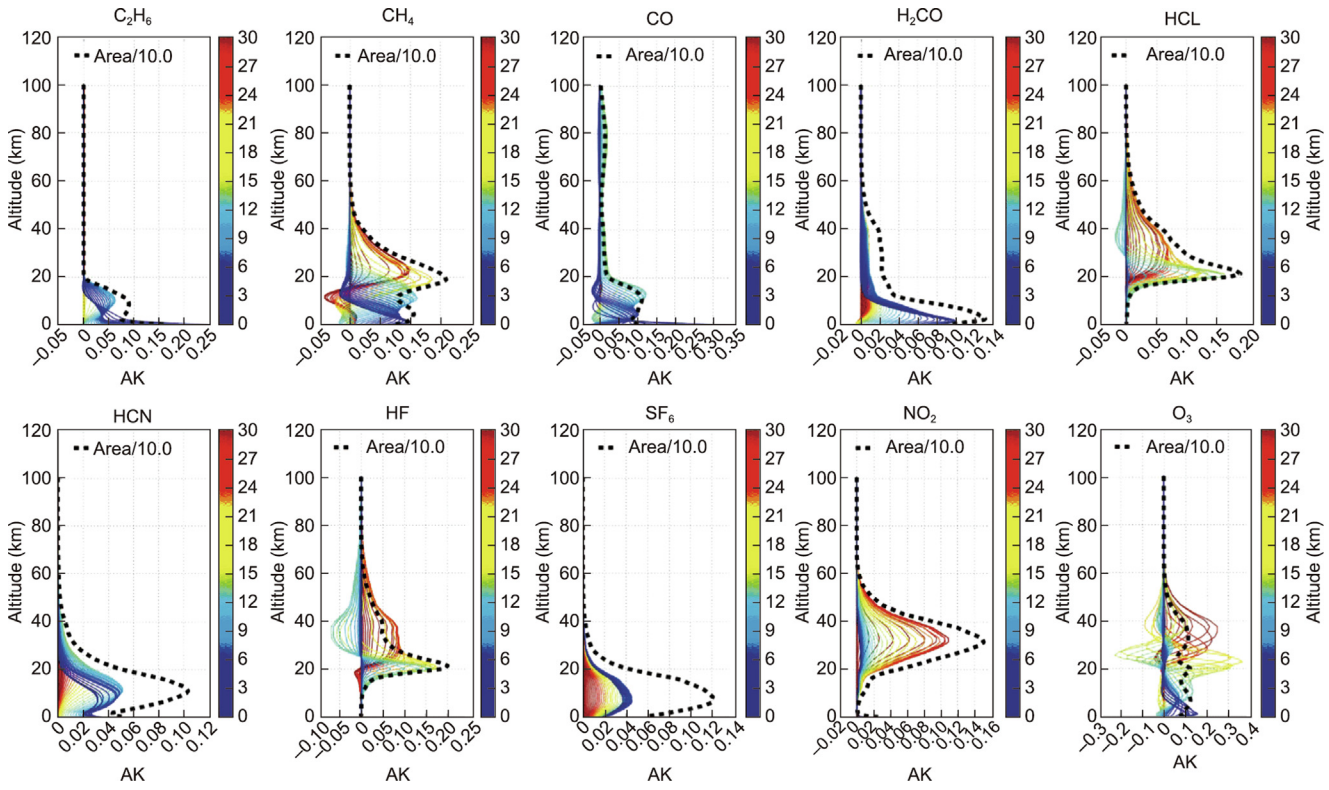

Fig. 4. AKs (colored fine lines) of some tropospheric (C_2H_6, CH_4, CO, H_2CO, HCN, and SF_6) and stratospheric (HCl, HF, NO_2, and O_3) gases retrieved with the MIR spectra suite at the Hefei station. The area of AKs for each gas is plotted in a black dashed line and scaled by a factor of 0.1. Demonstrations for all gases are prescribed from randomly selected retrievals.

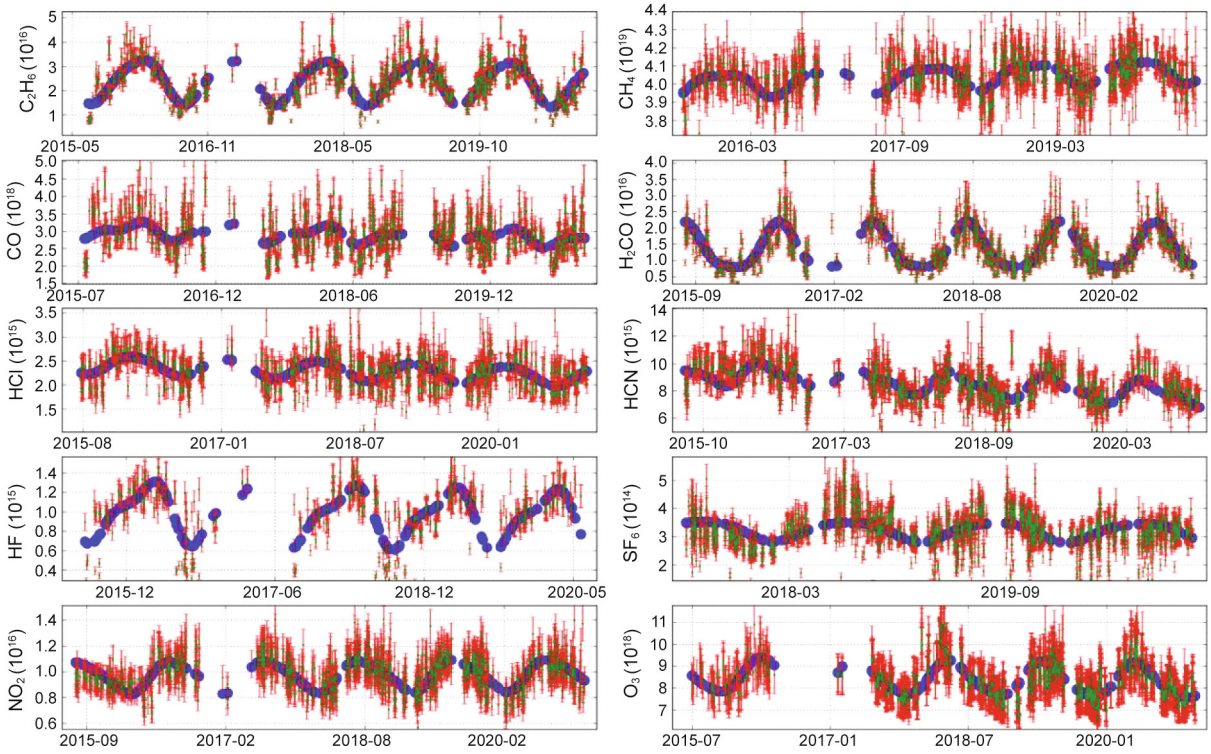

Fig. 5. Total column time series of some typical gases retrieved with the MIR spectra suite at the Hefei station. The seasonality of each gas (represented by blue dots) is fitted using a bootstrap resampling model with a third Fourier series. Vertical error bars represent retrieval uncertainties. The units of the *y*-coordinate are molecular·m^{-2}.

Table 2
Inventory of papers based on FTS observations at the Hefei station during 2014–2020, categorized by key findings, data period, theme (i.e., main gases considered), waveband, atmospheric domain, and topic.

Authors	Key findings	Period	Theme	Waveband	Domain	Topic
Wang et al. [62]	X_{CO_2} at the Hefei station showed an obvious seasonal cycle, but X_{CO} displayed no clear seasonality. X_{CO_2} observations at the Hefei station are in good agreement with both the Greenhouse gases observing satellite (GOSAT) and Orbiting Carbon Observatory-2 (OCO-2) observations	2014-06 to 2016-04	CO_2, CO	IR	Troposphere and stratosphere	Overall characteristics and satellite evaluation
Tian et al. [63]	Diurnal X_{CH_4} exhibits an increasing change rate in summer and shows a decreasing change rate or remains constant in other seasons. X_{CH_4} shows a seasonal maximum in summer and a minimum in winter. X_{CH_4} from 2014 to 2017 showed an increasing change rate of (0.56% ± 0.15%) a^{-1}	2014-06 to 2017-07	CH_4	IR	Troposphere and stratosphere	Retrieval harmonization, satellite evaluation, and model evaluation
Sun et al. [75]	Attenuators cause negligible ILS drifts and can be used to adapt the received intensity of the detector. The usage of different sizes of field stop may cause dramatic ILS drifts due to inconsistent mechanical errors among the selected field stops	2015	ILS	IR and MIR	Troposphere and stratosphere	ILS characterization
Sun et al. [73]	Tropospheric gases are less sensitive to ILS drift than stratospheric gases and, for the same level of drift, the negative ILS influence is smaller than the positive ILS. To limit the difference in the total column of $ClONO_2$ within 10% and other gases within 1%, upper limits of ILS for CH_4, N_2O, CO, HCN, C_2H_6, O_3, $ClONO_2$, HNO_3, HF, and HCl are suggested	2015-08 to 2016-08	CH_4, N_2O, CO, HCN, C_2H_6, O_3, $ClONO_2$, HNO_3, HF, HCl	MIR	Troposphere and stratosphere	ILS characterization and retrieval harmonization
Sun et al. [66]	The effect of ILS drift on the partial column is gas and altitude dependent. To suppress the influence on the partial column to within 2%, upper limits of ILS for CH_4, N_2O, O_3, and CO are suggested	2015-08 to 2016-08	CH_4, N_2O, O_3, CO	MIR	Troposphere and stratosphere	ILS characterization and retrieval harmonization
Sun et al. [8]	The level and variability of tropospheric O_3 in spring and summer (March–April–May/June–July–August; MAM/JJA) are higher than those in autumn and winter (September–October–November/December–January–February (SON/DJF). Reductions in volatile organic compounds (VOCs) and NO_x could effectively mitigate O_3 pollution in the SON/DJF and MAM/JJA seasons, respectively	2014-09 to 2017-09	O_3	MIR	Troposphere	Overall characteristics and source attribution
Shan et al. [76]	CO emissions over the megacity Hefei are calculated by utilizing the enhancement $\Delta CO/\Delta CO_2$ ratios derived from the NIR measurements at the Hefei station. The discrepancy between the CO emissions inferred from emission inventories and those from the measurements is also investigated	2015-09 to 2017-08	CO	IR	Troposphere	Emission estimates
Yin et al. [71]	Stratospheric NO_2 column at the Hefei station shows a seasonal maximum in June and a minimum in January. GEOS-Chem model can simulate the burden, seasonal cycle, and interannual trend of stratospheric NO_2 over the polluted east China	2015-07 to 2019-01	NO_2	MIR	Stratosphere	Overall characteristics, satellite evaluation, and model evaluation
Hedelius et al. [77]	FTS measurements at the Hefei station can be used as one of the reference datasets for the evaluation of measurements of pollution in the troposphere (MOPITT) X_{CO} version 7 retrievals	2015-09 to 2016-12	CO	NIR	Troposphere and stratosphere	Satellite evaluation
Yin et al. [78]	HCl total column at the Hefei station shows a seasonal maximum in January and a minimum in September. GEOS-Chem model can simulate the burden, seasonal cycle, and interannual trend of stratospheric HCl over the polluted east China.	2015-07 to 2019-04	HCl	MIR	Troposphere and stratosphere	Overall characteristics and model evaluation
Oshio et al. [79]	FTS measurements at the Hefei station can be used as one of the reference datasets for bias correction of the CH_4/CO_2 total column ratio retrieved from GOSAT observations	2015-09 to 2016-12	CO_2, CH_4	NIR	Troposphere and stratosphere	Satellite evaluation
Sun et al. [10]	Tropospheric columns of HCN at the Hefei station show pronounced seasonal variations with three seasonal peaks in May, September, and December, respectively. Elevated BB emissions in Oceania dominated the HCN enhancements in the second half of 2015. Elevated BB emissions in SEAS dominated the HCN enhancements in the first half of 2016	2015 to 2018	HCN	MIR	Troposphere	Overall characteristics, model evaluation, and source attribution
Shan et al. [80]	GEOS-Chem model can simulate the burden, seasonal cycle, and interannual trend of CO_2 over the polluted eastern China	2015-07 to 2019-12	CO_2	NIR	Troposphere	Overall characteristics and model evaluation
Sun et al. [13]	H_2CO photolysis plays a significant role in OH generation over east China. Non-methane volatile organic compound (NMVOC)-related summertime H_2CO enhancements were largely caused by NMVOC emissions within east China. Due to the increase in photochemical H_2CO resulting from increases in both NMVOCs and CH_4, H_2CO from 2015 to 2019 showed an increasing trend	2015 to 2019	H_2CO	MIR	Troposphere and stratosphere	Overall characteristics, model evaluation, and source attribution

(*continued on next page*)

Table 2 (*continued*)

Authors	Key findings	Period	Theme	Waveband	Domain	Topic
Sun et al. [15]	The observed C_2H_6 variability at the Hefei station was mainly driven by the variation of C_2H_6 emissions within China. The decrease in C_2H_6 from 2015 to 2020 points to improving air quality in China, due to a reduction in transported and local C_2H_6 emissions in recent years	2015 to 2020	C_2H_6	MIR	Troposphere	Overall characteristics, model evaluation, and source attribution
Yin et al. [67]	The X_{HF} time series at the Hefei station reached a seasonal maximum in March and a minimum in September. HF columns showed a decreasing change rate of (−0.38% ± 0.22%) a^{-1} between 2015 and 2020	2015 to 2020	HF	MIR	Stratosphere	Overall characteristics and retrieval harmonization
Shan et al. [81]	The stratospheric HNO_3 column at the Hefei station reached a seasonal maximum in March and a minimum in September, and showed a decreasing change rate of (−9.45% ± 1.20%) a^{-1} between 2017 and 2019	2017 to 2019	HNO_3	MIR	Stratosphere	Overall characteristics and satellite evaluation

4.1. ILS characterization and retrieval harmonization

Most FTS stations within the TCCON/NDACC networks utilize different sizes of field stop or attenuators to adapt the received optical intensity of the detector. These behaviors may modify the ILS of a high-resolution FTS spectrometer, which can cause retrieval biases if the resulting ILS drifts are not properly addressed. Sun et al. [75] first quantified the ILS drifts of a high-resolution FTS spectrometer with respect to different kinds of attenuators. They inserted five attenuators in front of or behind the interferometer and conducted ILS measurements to monitor the ILS of the high-resolution FTS instrument. Sun et al. [75] concluded that any of the five attenuators caused negligible ILS drifts and could be used to adapt the received optical intensity of the detector. However, the usage of different sizes of field stop may cause dramatic ILS drifts due to inconsistent mechanical errors among the selected field stops.

Sun et al. [66,73] further simulated different kinds of ILS drifts and quantified their effect on the retrieval of all NDACC gases. The sensitivities of the total column and partial column to different levels of ILS drift were investigated. Sun et al. found that the tropospheric gases are less sensitive to ILS drift than the stratospheric gases; furthermore, for the same level of drift, the negative ILS influence is smaller than the positive ILS. For an ILS drift of 10%, the total columns of CH_4, N_2O, CO, HCN, C_2H_6, O_3, $ClONO_2$, HNO_3, HF, and HCl changed by 0.04%, 0.20%, 2.10%, 0.75%, 1.10%, 1.90%, 23.00%, 0.70%, 3.00%, and 4.00%, respectively [73]. To limit the difference in the total column of $ClONO_2$ within 10% and those of the other gases within 1%, the upper limits of positive ILS drifts for O_3, $ClONO_2$, HNO_3, HF, HCl, CO, HCN, and C_2H_6 are 6%, 5%, 15%, 5%, 5%, 5%, 13%, and 9%, respectively; the upper limits of negative ILS drifts for O_3, HF, and HCl are 6%, 12%, and 12%, respectively; and the influence of ILS drift for CH_4 and N_2O is negligible [73].

Sun et al. [66] concluded that the effect of ILS drift on a partial column is gas and altitude dependent. The influences of ILS drift on CH_4 and N_2O are smaller than those on O_3 and CO. In order to suppress the influence on a partial column within 2%, it is suggested that a precise ILS be used for CO and O_3. For CH_4, the upper limits of the positive ILS drift for altitude ranges of 0–7 and 16–37 km are 13.0% and 1.5%, respectively. The upper limits of the negative ILS drift for altitude ranges of 7–16 and 16–37 km are 12.0% and 4.5%, respectively. The influence of the negative ILS drift on the partial column of CH_4 at 0–7 km and that of the positive ILS drift at 7–16 km are negligible [66]; for N_2O, the upper limits of the positive ILS drift for altitude ranges of 0–5.0, 5.0–11.5, 11.5–20.0, and 20.0–35.0 km are 6.0%, 4.0%, 1.5%, and 1.5%, respectively. The upper limits of the negative ILS drift for altitude ranges of 11.5–20.0 and 20.0–35.0 km are 2.0% and 1.5%, respectively. However, the influence of the negative ILS drift on partial columns of N_2O at 0–5.0 and 5.0–11.5 km are negligible [66].

The NIR and MIR spectra at the Hefei station were collected with different optical filters, beam splitters, and detectors and were retrieved with different Micro-windows (MWs), spectral modeling schemes, and iterative methods, which could result in retrieval biases. In order to determine whether the NIR and MIR HF datasets at the Hefei station can be combined into a single reliable dataset, Yin et al. [67] compared these two datasets and identified their discrepancies. They found that the NIR and MIR X_{HF} data exhibit consistent seasonality, but the daily mean values of NIR X_{HF} are generally lower than the MIR data, with an average difference of (6.90 ± 1.07) parts per trillion by volume (pptv) [67]. As a result, Yin et al. [67] added a bias of 6.90 pptv to the NIR dataset before combining these two datasets for investigation.

Inconsistent field stops and detectors were used for the NIR spectra in the early stage of operation. These NIR spectra also lacked synchronous meteorological data and were subject to timing errors due to an incomplete observation protocol. All these

observation deficiencies would cause biases between individual measurements if not properly treated. In order to obtain a consistent long-term X_{CH_4} time series, Tian et al. [63] conducted a series of corrections to eliminate these potential biases and applied a bias of 11.0 ppb to the X_{CH_4} dataset derived before July 2015 [63].

4.2. Overall characteristics of key atmospheric constituents

We have conducted several works using the continuous FTS observations at the Hefei station to investigate the overall characteristics of the key atmospheric constituents over east China. Wang et al. [62] first investigated the seasonal cycles of CO_2 and CO with two year NIR measurements at the Hefei station. Wang et al. [62] found that the FTS time series of X_{CO_2} showed an obvious seasonal cycle, while the time series of X_{CO} displayed no clear seasonality. The researchers further analyzed the relationship between X_{CO} and X_{CO_2}, and found that these two species were only correlated for individual days and varied according to prevailing wind conditions. The correlation slopes of these two species in Hefei are usually smaller than those in Beijing, indicating that the two megacities have different emission characteristics. Tian et al. [63] reported an increasing change rate of (0.56% ± 0.15%) a^{-1} in X_{CH_4} based on three years' worth of NIR observations at the Hefei station (2014–2017). Diurnal X_{CH_4} generally exhibited an increasing change rate in summer (June–July–August; JJA) and showed a decreasing change rate or remained constant in other seasons. The X_{CH_4} time series show seasonal maxima in JJA and minima in winter (December–January–February; DJF). The X_{CH_4} annual means in January were 30–55 ppb lower than those in August.

Sun et al. [8,10,13,15] investigated the seasonality and interannual trends of O_3, HCN, H_2CO, and C_2H_6 over east China using different time scales of MIR observations at the Hefei station. Tropospheric O_3 (0–12 km) was shown to be characterized by a seasonal maximum in June and minimum in December [8]. Tropospheric columns of O_3 in June were 50% higher than those in December. The day-to-day variabilities of tropospheric O_3 in spring (March–April–May; MAM) and JJA were generally larger than those in autumn (September–October–November; SON) and DJF, and a broad high-value range within MAM/JJA was observed. These findings differ from those of Vigouroux et al. [82], who showed that tropospheric columns of O_3 at relatively clean sites usually reach a seasonal maximum in springtime.

The tropospheric columns (0–15 km) of HCN at the Hefei station showed pronounced seasonal variations, with three seasonal peaks in May, September, and December, respectively [10]. The tropospheric column of HCN was characterized by a seasonal maximum in May and minimum in November. In general, the tropospheric columns of HCN at the Hefei station are higher than the FTS observations at the NDACC sites arrival heights (78°S), Lauder (45°S), Reunion Maido (21°S), Mauna Loa (20°N), Izana (28°N), Rikubetsu (43°N), Toronto (44°N), Jungfraujoch (47°N), Bremen (53°N), Kiruna (68°N), and Ny Alesund (79°N). The tropospheric columns of HCN between September 2015 and July 2016 were 5%–46% larger than those during the same period in other years.

The X_{H_2CO} time series at the Hefei station reached a seasonal maximum in July and a minimum in January [13]. The FTS X_{H_2CO} values in January were 42.9% lower than those in July. The variabilities of X_{H_2CO} at the Hefei station are in good agreement with those of surface H_2CO measurements; thus, the FTS column observations were applied as a representation of near-surface conditions by Sun et al. [13] for source separation. The X_{H_2CO} time series at the Hefei station showed a positive change rate of (2.37% ± 0.70%) a^{-1} from 2015 to 2019. In the studied years, Sun et al. [13] found that hydroxyl (OH) production from H_2CO photolysis was comparable with that from O_3 photolysis, indicating that H_2CO photolysis plays an important role in OH generation over east China.

Sun et al. [15] found that the tropospheric (0–12 km) column-averaged dry air mole fraction (troDMF) of C_2H_6 reached a seasonal maximum in December and a minimum in July, and showed a negative change rate of (−2.60% ± 1.33%) a^{-1} from 2015 to 2020. The C_2H_6 troDMF seasonality is characterized by a winter maximum and a summer minimum because the tropospheric OH oxidation capability in summer is higher than that in winter [15]. Both emission and meteorological factors have negative effects on C_2H_6 troDMF in JJA/SON and positive effects in DJF/MAM. Regional and long-range transport of C_2H_6 over east China is largely driven by the Asian monsoon and mid-latitude westerlies [15].

In addition to tropospheric gases, the seasonal and interannual variabilities of a few stratospheric gases have been investigated. Yin et al. [71] found that the stratospheric NO_2 columns at the Hefei station incrementally increase in the first half of the year and decrease in the second half of the year, with a seasonal maximum in June and a minimum in January. The stratospheric columns of NO_2 in June are on average 39.20% ± 8.95% higher than those in January. High values of summertime stratospheric NO_2 columns are attributed to a faster photolysis of N_2O_5 and HNO_3 by higher solar intensity in summer [71]. Further studies by Yin et al. [67,78] and Shan et al. [81] concluded that the seasonal cycles of HCl, HF, and HNO_3 in the stratosphere are associated with the variability of tropopause height. Stratospheric HCl, HF, and HNO_3 columns showed a seasonal maximum in January and a minimum in September [67,78,81]. Stratospheric NO_2, HCl, HF, and HNO_3 columns showed decreasing change rates of (−0.34% ± 0.05%) a^{-1} between 2015 and 2018, (−1.83% ± 0.13%) a^{-1} between 2015 and 2019, (−0.38% ± 0.22%) a^{-1} between 2015 and 2020, and (−9.45% ± 1.20%) a^{-1} between 2017 and 2019, respectively.

4.3. Emission estimates

For regions where CO and CO_2 share common sources, CO emission can be inferred by studying the correlation between CO and CO_2. Shan et al. [76] utilized the enhancement $\Delta CO/\Delta CO_2$ ratios derived from the NIR measurements at the Hefei station to calculate the CO emission over the megacity Hefei. They also investigated the discrepancy between the CO emissions inferred from emission inventories and those from the measurements. In order to do so, the researchers compared the enhancement $\Delta CO/\Delta CO_2$ ratios at the Hefei station derived from FTS, satellite, *in situ* measurement, and emission inventory from September 2015 to August 2017. The Emission Database for Global Atmospheric Research (EDGAR) emission inventories and the Peking University (PKU) emission inventories were used in the study. Shan et al. [76] concluded that the two emission inventory-based $\Delta CO/\Delta CO_2$ ratios are substantially larger than those based on measurements from ground-based FTS, *in situ* instruments, and satellite. Furthermore, the error bars of the emission inventory-based $\Delta CO/\Delta CO_2$ ratios are higher than those based on measurements, indicating that the $\Delta CO/\Delta CO_2$ ratios derived from the two emission inventories have high uncertainties [76].

Shan et al. [76] further used the FTS-based $\Delta CO/\Delta CO_2$ ratio and the CO_2 emissions derived from the EDGAR and PKU inventories to infer CO emissions. The CO emissions calculated with the EDGAR inventory-based CO_2 emissions and the ground-based FTS $\Delta CO/\Delta CO_2$ ratios were about (11.27 ± 0.91) $Tg{\cdot}a^{-1}$ for 2015–2016 and (12.35 ± 0.74) $Tg{\cdot}a^{-1}$ for 2016–2017. The CO emissions during the same periods estimated from the PKU inventory-based CO_2 emissions and the ground-based FTS $\Delta CO/\Delta CO_2$ ratios were about (10.96 ± 0.88) and (11.95 ± 0.71) $Tg{\cdot}a^{-1}$, respectively. As the PKU and EDGAR inventories can well reproduce actual CO_2 emissions, the CO emissions calculated with the two inventory-based CO_2 emissions and the FTS $\Delta CO/\Delta CO_2$ ratios are in good agreement. However, Shan et al. [76] observed a large discrepancy between

the CO emissions derived from the emission inventories and those derived from ground-based FTS observations. The CO emissions estimated from the EDGAR inventory are 19.12 and 17.88 Tg·a^{-1}, while those from the PKU inventory are 38.07 and 35.60 Tg·a^{-1} for 2015–2016 and 2016–2017, respectively. This finding indicates that both emission inventories substantially overestimated the real CO emissions near Hefei.

4.4. Evaluating satellite observations

The continuous FTS observations at the Hefei station provide a series of valuable datasets that can be used to validate satellite observations. To compare the measurements obtained from satellites and ground-based FTS, their differences in vertical resolution and the *a priori* profile are considered. First, the satellite data are re-gridded to the FTS *a priori* profile to minimize the *a priori* profile-associated difference [56]. The FTS data are then smoothed by the concurrent satellite AKs to minimize the vertical resolution-associated difference. Finally, the re-gridded and smoothed datasets of these two observations are compared.

Wang et al. [62] found that the ground-based FTS X_{CO_2} time series at the Hefei station are in good agreement with both the greenhouse gases observing satellite (GOSAT) and Orbiting Carbon Observatory-2 (OCO-2) observations [62]. Compared with the ground-based FTS observations, the daily median of the GOSAT and OCO-2 X_{CO_2} time series from 2015 to 2017 have biases of (−0.52 ± 1.63) and (0.81 ± 1.73) ppm, respectively. The GOSAT and OCO-2 observations can reproduce the daily median of FTS X_{CO_2} time series with a correlation coefficient (r) of 0.79 and 0.83, respectively. Tian et al. [63] observed that the differences between the GOSAT and FTS X_{CH_4} data at the Hefei station (GOSAT−FTS) were within the error budgets of both datasets and were season independent, with a mean value of (1.6 ± 13.0) ppb (0.09% ± 0.70%). This mean difference is comparable to similar comparisons at other TCCON sites [50,83]. The seasonal cycles of X_{CH_4} observed by GOSAT and FTS are in good agreement with a correlation coefficient (r) of 0.77.

Yin et al. [71] found that the stratospheric NO_2 time series from 2015 to 2018 observed by the ozone monitoring instrument (OMI) satellite are in good agreement with the concurrent ground-based FTS data at the Hefei station. The seasonal cycles of stratospheric NO_2 observed by OMI and FTS are correlated with a correlation coefficient (r) of 0.841 [71]. The annual mean difference between OMI and FTS (OMI − FTS) is (1.48 ± 5.33) × 10^{14} molecules·cm^{-2} (4.82% ± 17.37%) [71], which is within the uncertainties of both datasets. The OMI versus FTS differences in MAM are higher than those in the other seasons. Yin et al. [71] also found that the negative stratospheric NO_2 trend between 2015 and 2018 obtained by OMI observations (−0.91% ± 0.09%) a^{-1} is consistent with that obtained by ground-based FTS. The FTS measurements at Hefei station have also been used by Oshio et al. [79] as one of the reference datasets for the bias correction of the CH_4/CO_2 total column ratio retrieved from GOSAT observations and by Hedelius et al. [77] for the evaluation of measurements of pollution in the troposphere (MOPITT) X_{CO} v7 retrievals.

The stratospheric HNO_3 and HCl columns at the Hefei station were compared with Microwave Limb Sounder (MLS) satellite data. Shan et al. [81] found that MLS satellite data showed similar seasonal variations and annual rates as the Fourier-transform infrared (FTIR) data, and that the stratospheric HNO_3 and HCl columns of the two datasets have correlation coefficients (r) of 0.87 and 0.88, respectively. The mean bias between the satellite and FTIR data of the stratospheric HNO_3 and HCl columns is −8.58% ± 12.22% and 4.58% ± 13.09%, respectively.

The results from Wang et al. [62], Tian et al. [63], Yin et al. [71], Hedelius et al. [77], Oshio et al. [79], and Shan et al. [81] have verified the ability of the ground-based FTS observations at the Hefei station to detect diurnal, seasonal, and interannual variabilities of key atmospheric constituents in both the troposphere and stratosphere and to validate satellite observations.

4.5. Evaluating CTM simulations

Several studies have been conducted with the continuous FTS observations at the Hefei station to evaluate the performance of CTM in the polluted region of east China. Since the vertical resolution of CTM differs from the ground-based FTS observations, a smoothing correction is applied to the model profiles [84]. First, the model profiles are re-gridded to the FTS height grid to reconcile a common height grid. The re-gridded profiles are then smoothed by *a priori* profiles and the concurrent AKs of FTS [68,84]. Subsequently, the smoothed model profiles are converted to a total column or DMF using the concurrent re-gridded air density profiles from the CTM. Finally, the converted CTM data are compared with the ground-based FTS data.

The FTS time series of many gases, such as CH_4, NO_2, H_2CO, C_2H_6, and CO_2, obtained at the Hefei station have been used to validate the GEOS-Chem model. In general, GEOS-Chem simulations can reproduce the seasonal cycles and interannual trends of the gases observed by ground-based FTS. The correlation coefficients (r) between GEOS-Chem and the FTS for X_{CH_4}, the stratospheric column of NO_2, X_{H_2CO}, the C_2H_6 troDMF, and the CO_2 troDMF are 0.860, 0.8580, 0.780, 0.880, and 0.890, respectively [13,15,63,71,80]. However, the observed day-to-day variabilities of these gases cannot always be reproduced by the GEOS-Chem model [13]. For example, the GEOS-Chem versus FTS differences for X_{CH_4} in JJA are 35–55 ppb larger than those in DJF [63]. For the stratospheric column of NO_2, the differences in SON are smaller than those in other seasons [71]. For the C_2H_6 troDMF, the observed monthly mean values are overestimated by 35.6% in July and underestimated by 17.4% in December by the GEOS-Chem model [15]. These discrepancies can mostly be attributed to uncertainties in the vertical mixing and horizontal transport schemes simulated by the GEOS-Chem model at a coarse spatial resolution, which make it difficult to match column observation over a single point. In particular, the Hefei station is located in a highly industrialized and densely populated region in east China. The regional differences in the atmospheric burdens of these gases could affect the comparison with the FTS observations. In addition, the differences between simulation and measurement could be associated with the uncertainties in emission inventories and chemical mechanisms. For example, many oxidation pathways of volatile organic compounds (VOCs) may not be optimally implemented or may not even be considered in the GEOS-Chem model. Furthermore, the geographical distributions of various emission sources and how these sources affect the air masses over the polluted Hefei station may not always be properly addressed in the model.

Nevertheless, the GEOS-Chem versus FTS differences for X_{CH_4}, the stratospheric column of NO_2, X_{H_2CO}, the C_2H_6 troDMF, and the CO_2 troDMF are (−8.09 ± 17.83) ppb (0.45% ± 0.95%), (2.36 ± 2.33) × 10^{14} molecules·cm^{-2} (7.66% ± 7.49%), (−0.05 ± 0.20) ppbv (−2.60% ± 10.40%), (−0.02 ± 0.05) ppbv (−1.60% ± 4.20%), and (−1.68 ± 1.23) ppbv (−0.42% ± 0.31%), respectively, which are within the FTS uncertainty budget of the respective gases. These results verify that GEOS-Chem can simulate the burdens, seasonal cycles, and interannual trends of CH_4, NO_2, H_2CO, C_2H_6, and CO_2 over the polluted east China [13,15,63,71,80].

4.6. Air pollution, sources, and transport

With tropospheric columns of O_3, H_2CO, and CO provided by FTS, the tropospheric column of NO_2 provided by OMI, and

the air mass trajectories, Sun et al. [8] investigated the O_3 photochemical regime at the Hefei station. Sun et al. concluded that the emissions in the Shandong and Hebei Provinces in north China, the Jiangsu and Anhui Provinces in east China, the Shaanxi, Hubei, and Hunan Provinces in central China, and the Henan and Shanxi Provinces in northwest China contribute to the O_3 burdens at the Hefei station [8]. The level and variability of tropospheric O_3 in MAM/JJA are higher than those in SON/DJF because air masses in MAM/JJA have a stronger tendency to originate from highly industrialized and densely populated regions. Sun et al. [8] further used the H_2CO/NO_2 tropospheric column ratio as a proxy to explore the photochemical production sensitivity of O_3 (PO_3), and found that the temporal PO_3 during the measurement time is mainly limited to NO_x in MAM/JJA and is limited to VOCs or mixed VOCs–NO_x in SON/DJF. Emissions control for VOC and NO_x could effectively mitigate O_3 pollution in the SON/DJF and MAM/JJA seasons, respectively [8].

The GEOS-Chem model captured the observed variabilities of CO, H_2CO, and C_2H_6 at the Hefei station and was thus used for source attributions of these gases by Sun et al. [10,13,15]. Sun et al. [10] found that the enhancements of tropospheric HCN (ΔHCN) and CO (ΔCO) are correlated, which indicates that the CO and HCN enhancements in the troposphere can be attributed to the same sources [10]. Taking this advantage, Sun et al. [10] used GEOS-Chem-tagged CO simulation to determine the source of HCN and concluded that the seasonal maximum of HCN in May can be mainly attributed to BB emissions in SEAS (41.0% ± 13.1%), Africa (AF) (22.0% ± 4.7%), and Europe and boreal Asia (EUBA) (21.0% ± 9.2%). The seasonal maximum of HCN in September can be mainly attributed to BB emissions in EUBA (38.0% ± 11.3%), SEAS (14.0% ± 3.3%), AF (26.0% ± 6.7%), and North America (NA) (13.7% ± 8.3%). With respect to the seasonal maximum of HCN in December, dominant influences are from AF (36.0% ± 7.0%), NA (18.7% ± 5.2%), and EUBA (21.0% ± 5.2%). The enhanced tropospheric columns of HCN between 2015 and 2016 were due to elevated BB emissions in SEAS, Oceania (OCE), and EUBA during that period. More specifically, the elevated BB emissions in OCE dominated the HCN enhancements in the second half of 2015, while elevated BB emissions in SEAS dominated the HCN enhancements in the first half of 2016 [10].

Sun et al. [13] used the GEOS-Chem model to quantify the contributions of different geographical regions and emission categories to the summertime H_2CO enhancements at the Hefei station [13]. The results showed that the oxidation of nonmethane volatile organic compound (NMVOCs) and CH_4 caused the summertime H_2CO enhancements over Hefei, with contributions of 56.73% and 43.27%, respectively. The NMVOC-related summertime H_2CO enhancements were largely caused by NMVOC emissions in east China. Due to the increase in photochemical H_2CO resulting from increases in both NMVOCs and CH_4, H_2CO emissions from 2015 to 2019 showed an increasing trend [13]. With similar sensitivity simulations as those used in their earlier work [13], Sun et al. [15] concluded that anthropogenic (biofuel plus fossil fuel) emissions accounted for 49.2% and natural (BB plus biogenic) emissions accounted for 37.0% of the C_2H_6 burden over east China. The observed C_2H_6 variability at the Hefei station was mainly driven by the variation in C_2H_6 emissions within China (74.0%), where north, east, and central China accounted for most of the contribution (57.6%). A decrease in C_2H_6 from 2015 to 2020 points to an improvement in the air quality in China, which can be attributed to a reduction in transported and local C_2H_6 emissions in recent years [15].

5. Conclusion and future outlook

This study summarized the major achievements obtained from the long-term observations of atmospheric constituents at the first ground-based high-resolution FTS station in China, which has been located in Hefei, east China, since 2014. These results have improved our current knowledge on the retrieval and characterization of high-resolution spectra, climate change, emission estimates, satellite and CTM validations, and the sources and transport of atmospheric pollution. New findings on physical processes and chemical mechanisms will be implemented into CTMs in the near future. In turn, the validated CTMs and the measurement data will be used to further understand the impact of atmospheric production and depletion processes on a larger scale. Based on these achievements and the overall envisaged concept of this station, the following scientific studies are expected to be conducted at the Hefei station in future.

(1) In order to use ground-based total column or profile retrievals to investigate different scales of atmospheric research and provide a standard transfer among different observation platforms, the ground-based FTS dataset must be converted to the same validation scale as the World Meteorological Organization (WMO) scale. We have not yet validated the ground-based FTS data at Hefei to *in situ* profile measurements based on airborne instruments. Such a comparison will enhance the accuracy level of the ground-based FTS observations. At present, we simply assume that the calibration value that is valid for other TCCON sites is also valid for Hefei, and scale our NIR observations by the observed biases reported by Wunch et al. [17]. Therefore, we look forward to using airborne profile measurements to further improve the accuracy of the observations.

(2) To understand the interaction between atmospheric constituents and climate change, long-term measurements of a sufficient number of atmospheric constituents are needed. Therefore, trend-quality stable measurements of all atmospheric constituents at the Hefei station will be continued. A few more species will be investigated, such as PAN, OCS, NH_3, and chloro–fluoro–carbons (CFCs); this list of species will continue to increase over time, in keeping with the evolution of the retrieval techniques and new spectral data. Unlike other spectrometers within the TCCON/NDACC networks, the IFS125HR used at the Hefei station covers the UV spectral range; however, we have not attempted to collect UV spectra in routine observations. We plan to collect UV spectra in future, which will further increase the number of atmospheric constituents. In order to contribute to the mitigation of climate change, China has explicitly proposed reaching a peak in its CO_2 emissions by 2030 and realizing carbon neutrality by 2060. The Hefei station will provide scientific assistance for the Chinese Government to develop green economy policies and to achieve carbon neutrality and the goals of the Paris Agreement.

(3) As a part of the AEOS infrastructure, the high accuracy of the FTS dataset will allow it to be used extensively to validate other instruments within the AEOS framework and above. Despite their outstanding capabilities in precision and stability, IFS125HR spectrometers have limitations. The IFS125HR is an expensive and ponderous spectrometer, and its operation requires a significant amount of infrastructure. Furthermore, it is difficult and time consuming to regularly maintain its optical alignment. To overcome these problems, the usage of smaller, cheaper, and more easily transportable spectrometers such as the EM27/SUN and the VERTEX-80/SUN was recently investigated. Both the EM27/SUN and the VERTEX-80/SUN have been verified to have similar features as the IFS125HR for certain gases (e.g., CO_2, CO, and H_2CO) but have better mobility [70,85]. The high accuracy of the FTS dataset will be used to validate the flexible instruments EM27/SUN and VERTEX-80/SUN before they are used to calculate the emission flux of a city or industrial facility. The validated EM27/SUN and VERTEX-80/SUN observations can then complement the existing high-resolution FTS observation dataset in China. The FTS dataset will be also used to validate the envisaged Chinese environmental satellites in future.

(4) The Hefei station has archived almost seven years of high-quality data for many atmospheric constituents. These data will be used together with the measurements from other platforms or CTM simulations and will continue to be available to the community in order to help us better understand climate change, air pollution, pollution sources and transport, and their impacts on crops and human health in China and around the world.

(5) The achievements made at the Hefei station have benefited from the close cooperation between AIOFM-CAS and the TCCON/NDACC networks. It is planned for the Hefei station to be more involved in international TCCON/NDACC observations and scientific activities, which will contribute to an understanding of the carbon cycle and climate change on a global scale.

(6) New spectroscopic properties will be studied with the high spectral resolution and precision of the ground-based FTS datasets at the Hefei station. These analyses of the spectral lines will improve the retrieval precision and accuracy of all kinds of observations at the Hefei station. We will collaborate with the spectroscopic community to improve the interpretation of atmospheric absorption and extinction.

Finally, the achievements based on our work at the Hefei station exemplify how a new station can improve the current understanding of climate change, air pollution, and pollution transport both on a regional scale and globally. Considering that humankind is facing the unprecedented challenge of climate change, it is necessary to build more stations of this kind in different regions around the globe—especially in Africa, South America, and Asia, where only sparse ground-based observations are available. It is only with sufficient measurements and close cooperation between all sites that we can better understand the atmosphere and predict the "future climate" using climate models.

Acknowledgments

This work is supported by the Youth Innovation Promotion Association, Chinese Academy of Sciences (CAS) (2019434) and the Sino–German Mobility programme (M-0036). We thank the NDACC/TCCON networks for providing the state-of-the-art software. We thank David Griffith and Nicholas Jones from university of Wollongong, James Hannigan from National Center for Atmospheric Research (NCAR), Thomas Blumenstock and Frank Hase from Karlsruhe Institute of Technology (KIT), Corinne Vigouroux from Royal Belgian Institute for Space Aeronomy, Emmanuel Mahieu from University of Liège, and many other colleagues within NDACC/TCCON networks for their help in setting up/operating the FTS spectrometer or analyzing the spectra at the Hefei station.

Compliance with ethics guidelines

Cheng Liu, Youwen Sun, Changgong Shan, Wei Wang, Justus Notholt, Mathias Palm, Hao Yin, Yuan Tian, Jixi Gao, and Huiqin Mao declare that they have no conflict of interest or financial conflicts to disclose.

Authors' contribution

Cheng Liu and Youwen Sun designed and wrote the paper with inputs from all coauthors. Changgong Shan is in charge of TCCON retrieval, analysis, and plotting. The rest of the authors contributed to this work by providing constructive comments.

Appendix A. Supplementary data

Supplementary data to this article can be found online at https://doi.org/10.1016/j.eng.2021.11.022.

Data availability

Dataset retrieved from the NIR spectra suite is archived in the TCCON database https://tccondata.org/. Dataset retrieved from the MIR spectra suite can be available from https://doi.org/10.5281/zenodo.5205257. Data format and usage of the NIR and MIR datasets at the Hefei station follow the TCCON and NDACC conventions, respectively.

References

[1] Sun YW, Liu C, Chan KL, Xie PH, Liu WQ, Zeng Y, et al. Stack emission monitoring using non-dispersive infrared spectroscopy with an optimized nonlinear absorption cross interference correction algorithm. Atmos Meas Tech 2013;6(8):1993–2005.
[2] Sun Y, Liu C, Xie P, Hartl A, Chan K, Tian Y, et al. Industrial SO_2 emission monitoring through a portable multichannel gas analyzer with an optimized retrieval algorithm. Atmos Meas Tech 2016;9(3):1167–80.
[3] Chan CK, Yao X. Air pollution in mega cities in China. Atmos Environ 2008;42(1):1–42.
[4] Ding A, Nie W, Huang X, Chi X, Sun J, Kerminen VM, et al. Long-term observation of air pollution–weather/climate interactions at the SORPES station: a review and outlook. Front Environ Sci Eng 2016;10(5):15.
[5] He KB, Huo H, Zhang Q. Urban air pollution in China: current status, characterizes and progress. Annu Rev Energy Environ 2002;27:397–431.
[6] Huang RJ, Zhang Y, Bozzetti C, Ho KF, Cao JJ, Han Y, et al. High secondary aerosol contribution to particulate pollution during haze events in China. Nature 2014;514(7521):218–22.
[7] Richter A, Burrows JP, Nüss H, Granier C, Niemeier U. Increase in tropospheric nitrogen dioxide over China observed from space. Nature 2005;437(7055):129–32.
[8] Sun Y, Liu C, Palm M, Vigouroux C, Notholt J, Hu Q, et al. Ozone seasonal evolution and photochemical production regime in the polluted troposphere in eastern China derived from high-resolution Fourier transform spectrometry (FTS) observations. Atmos Chem Phys 2018;18(19):14569–83.
[9] Xu X, Lin W, Wang T, Yan P, Tang J, Meng Z, et al. Long-term trend of surface ozone at a regional background station in eastern China 1991–2006: enhanced variability. Atmos Chem Phys 2008;8(10):2595–607.
[10] Sun Y, Liu C, Zhang L, Palm M, Notholt J, Yin H, et al. Fourier transform infrared time series of tropospheric HCN in eastern China: seasonality, interannual variability, and source attribution. Atmos Chem Phys 2020;20(9):5437–56.
[11] Zheng B, Tong D, Li M, Liu F, Hong C, Geng G, et al. Trends in China's anthropogenic emissions since 2010 as the consequence of clean air actions. Atmos Chem Phys 2018;18(19):14095–111.
[12] Lu X, Hong J, Zhang L, Cooper OR, Schultz MG, Xu X, et al. Severe surface ozone pollution in China: a global perspective. Environ Sci Technol Lett 2018;5(8):487–94.
[13] Sun Y, Yin H, Liu C, Zhang L, Cheng Y, Palm M, et al. Mapping the drivers of formaldehyde (HCHO) variability from 2015 to 2019 over eastern China: insights from Fourier transform infrared observation and GEOS-Chem model simulation. Atmos Chem Phys 2021;21(8):6365–87.
[14] Lu X, Zhang L, Chen Y, Zhou M, Zheng B, Li K, et al. Exploring 2016–2017 surface ozone pollution over China: source contributions and meteorological influences. Atmos Chem Phys 2019;19(12):8339–61.
[15] Sun Y, Yin H, Liu C, Mahieu E, Notholt J, Té Y, et al. The reduction in C_2H_6 from 2015 to 2020 over Hefei, eastern China, points to air quality improvement in China. Atmos Chem Phys 2021;21(15):11759–79.
[16] Hannigan J, Coffey M, Goldman A. Semiautonomous FTS observation system for remote sensing of stratospheric and tropospheric gases. J Atmos Ocean Technol 2009;26(9):1814–28.
[17] Wunch D, Toon GC, Wennberg PO, Wofsy SC, Stephens BB, Fischer ML, et al. Calibration of the total carbon column observing network using aircraft profile data. Atmos Meas Tech 2010;3(5):1351–62.
[18] De Mazière M, Thompson AM, Kurylo MJ, Wild JD, Bernhard G, Blumenstock T, et al. The network for the detection of atmospheric composition change (NDACC): history, status and perspectives. Atmos Chem Phys 2018;18(7):4935–64.
[19] Franco B, Mahieu E, Emmons LK, Tzompa-Sosa ZA, Fischer EV, Sudo K, et al. Evaluating ethane and methane emissions associated with the development of oil and natural gas extraction in North America. Environ Res Lett 2016;11(4):044010.
[20] Davis SP, Abrams MC, Brault JW. Fourier transform spectrometry. Cambridge: Academic Press; 2001.
[21] Messerschmidt J, Macatangay R, Notholt J, Petri C, Warneke T, Weinzierl C. Side by side measurements of CO_2 by ground-based Fourier transform spectrometry (FTS). Tellus B Chem Phys Meterol 2010;62(5):749–58.
[22] Wunch D, Toon GC, Blavier JF, Washenfelder RA, Notholt J, Connor BJ, et al. The total carbon column observing network. Philos Trans Royal Soc Math Phys Eng Sci 2011;369(1943):2087–112.
[23] Washenfelder RA. Column abundances of carbon dioxide and methane retrieved from ground-based near-infrared solar spectra [dissertation]. California: California Institute of Technology; 2006.

[24] Chevallier F, Deutscher NM, Conway TJ, Ciais P, Ciattaglia L, Dohe S, et al. Global CO_2 fluxes inferred from surface air-sample measurements and from TCCON retrievals of the CO_2 total column. Geophys Res Let 2011;38 (24):1–5.
[25] Deutscher NM, Sherlock V, Fletcher SE, Griffith DWT, Notholt J, Macatangay R, et al. Drivers of column-average CO_2 variability at Southern Hemispheric total carbon column observing network sites. Atmos Chem Phys 2014;14 (18):9883–901.
[26] Guerlet S, Basu S, Butz A, Krol M, Hahne P, Houweling S, et al. Reduced carbon uptake during the 2010 Northern Hemisphere summer from GOSAT. Geophys Res Lett 2013;40(10):2378–83.
[27] Keppel-Aleks G, Wennberg PO, Schneider T. Sources of variations in total column carbon dioxide. Atmos Chem Phys 2011;11(8):3581–93.
[28] Keppel-Aleks G, Wennberg PO, Washenfelder RA, Wunch D, Schneider T, Toon GC, et al. The imprint of surface fluxes and transport on variations in total column carbon dioxide. Biogeos 2012;9(3):875–91.
[29] Sussmann R, Forster F, Rettinger M, Bousquet P. Renewed methane increase for five years (2007–2011) observed by solar FTIR spectrometry. Atmos Chem Phys 2012;12(11):4885–91.
[30] Wunch D, Wennberg PO, Messerschmidt J, Parazoo NC, Toon GC, Deutscher NM, et al. The covariation of Northern Hemisphere summertime CO_2 with surface temperature in boreal regions. Atmos Chem Phys 2013;13(18):9447–59.
[31] Lutsch E, Dammers E, Conway S, Strong K. Long-range transport of NH_3, CO, HCN, and C_2H_6 from the 2014 Canadian Wildfires. Geophys Res Lett 2016;43 (15):8286–97.
[32] Viatte C, Strong K, Walker KA, Drummond JR. Five years of CO, HCN, C_2H_6, C_2H_2, CH_3OH, HCOOH and H_2CO total columns measured in the Canadian high Arctic. Atmos Meas Tech 2014;7:1547–70.
[33] Viatte C, Strong K, Hannigan J, Nussbaumer E, Emmons LK, Conway S, et al. Identifying fire plumes in the Arctic with tropospheric FTIR measurements and transport models. Atmos Chem Phys 2015;15(5):2227–46.
[34] Vigouroux C, Stavrakou T, Whaley C, Dils B, Duflot V, Hermans C, et al. FTIR time-series of biomass burning products (HCN, C_2H_6, C_2H_2, CH_3OH, and HCOOH) at Reunion Island (21°S, 55°E) and comparisons with model data. Atmos Chem Phys 2012;12(21):10367–85.
[35] Gordon IE, Kassi S, Campargue A, Toon GC. First identification of the a1Δg-X3Σg electric quadrupole transitions of oxygen in solar and laboratory spectra. J Quant Spectrosc Radiat Transf 2010;111(9):1174–83.
[36] Gordon IE, Rothman LS, Toon GC. Revision of spectral parameters for the B- and γ-bands of oxygen and their validation against atmospheric spectra. J Quant Spectrosc Radiat Transf 2011;112(14):2310–22.
[37] Hartmann JM, Tran H, Toon GC. Influence of line mixing on the retrievals of atmospheric CO_2 from spectra in the 1.6 and 2.1 μm regions. Atmos Chem Phys 2009;9(19):7303–12.
[38] Long DA, Hodges JT. On spectroscopic models of the O_2 A-band and their impact upon atmospheric retrievals. J Geophys Res 2012;117(D12):309.
[39] Miller CE, Wunch D. Fourier transform spectrometer remote sensing of O_2 A-band electric quadrupole transitions. J Quant Spectrosc Radiat Transf 2012;113 (11):1043–50.
[40] Reuter M, Bovensmann H, Buchwitz M, Burrows JP, Connor BJ, Deutscher NM, et al. Retrieval of atmospheric CO_2 with enhanced accuracy and precision from SCIAMACHY: validation with FTS measurements and comparison with model results. J Geophys Res 2011;116(D4):D04301.
[41] Reuter M, Bovensmann H, Buchwitz M, Burrows J, Deutscher N, Heymann J, et al. On the potential of the 2041–2047 nm spectral region for remote sensing of atmospheric CO_2 isotopologues. J Quant Spectrosc Radiat Transf 2012;113 (16):2009–17.
[42] Scheepmaker R, Frankenberg C, Galli A, Butz A, Schrijver H, Deutscher NM, et al. Improved water vapour spectroscopy in the 4174–4300 cm^{-1} region and its impact on SCIAMACHY HDO/H_2O measurements. Atmos Meas Tech 2013;6 (4):879–94.
[43] Tran H, Hartmann JM. An improved O_2 A band absorption model and its consequences for retrievals of photon paths and surface pressures. J Geophys Res 2008;113(D18):D18104.
[44] Tran H, Hartmann JM, Toon GC, Brown L, Frankenberg C, Warneke T, et al. The $2\nu_3$ band of CH_4 revisited with line mixing: consequences for spectroscopy and atmospheric retrievals at 1.67 μm. J Quant Spectrosc Radiat Transf 2010;111 (10):1344–56.
[45] Thompson DR, Benner DC, Brown LR, Crisp D, Malathy Devi V, Jiang Y, et al. Atmospheric validation of high accuracy CO_2 absorption coefficients for the OCO-2 mission. J Quant Spectrosc Radiat Transf 2012;113 (17):2265–76.
[46] Butz A, Guerlet S, Hasekamp O, Schepers D, Galli A, Aben I, et al. Toward accurate CO_2 and CH_4 observations from GOSAT. Geophys Res Lett 2011;38 (14):L14812.
[47] Boesch H, Deutscher NM, Warneke T, Byckling K, Cogan AJ, Griffith DWT, et al. HDO/H_2O ratio retrievals from GOSAT. Atmos Meas Tech 2013;6(3):599–612.
[48] Deng F, Jones D, Henze D, Bousserez N, Bowman K, Fisher J, et al. Inferring regional sources and sinks of atmospheric CO_2 from GOSAT X_{CO_2} data. Atmos Chem Phys 2014;14(7):3703–27.
[49] Frankenberg C, Wunch D, Toon G, Risi C, Scheepmaker R, Lee JE, et al. Water vapor isotopologue retrievals from high-resolution GOSAT shortwave infrared spectra. Atmos Meas Tech 2013;6(2):263–74.
[50] Morino I, Uchino O, Inoue M, Yoshida Y, Yokota T, Wennberg PO, et al. Preliminary validation of column-averaged volume mixing ratios of carbon dioxide and methane retrieved from GOSAT short-wavelength infrared spectra. Atmos Meas Tech 2011;4(6):1061–76.
[51] Oshchepkov S, Bril A, Yokota T, Yoshida Y, Blumenstock T, Deutscher NM, et al. Simultaneous retrieval of atmospheric CO_2 and light path modification from space-based spectroscopic observations of greenhouse gases: methodology and application to GOSAT measurements over TCCON sites. Appl Opt 2013;52 (6):1339–50.
[52] Parker R, Boesch H, Cogan A, Fraser A, Feng L, Palmer PI, et al. Methane observations from the Greenhouse Gases Observing Satellite: comparison to groundbased TCCON data and model calculations. Geophys Res Let 2011;38 (15):L15807.
[53] Reuter M, Bösch H, Bovensmann H, Bril A, Buchwitz M, Butz A, et al. A joint effort to deliver satellite retrieved atmospheric CO_2 concentrations for surface flux inversions: the ensemble median algorithm EMMA. Atmos Chem Phys 2013;13(4):1771–80.
[54] Schneising O, Bergamaschi P, Bovensmann H, Buchwitz M, Burrows JP, Deutscher NM, et al. Atmospheric greenhouse gases retrieved from SCIAMACHY: comparison to ground-based FTS measurements and model results. Atmos Chem Phys 2012;12(3):1527–40.
[55] Schepers D, Guerlet S, Butz A, Landgraf J, Frankenberg C, Hasekamp O, et al. Methane retrievals from Greenhouse Gases Observing Satellite (GOSAT) shortwave infrared measurements: performance comparison of proxy and physics retrieval algorithms. J Geophys Res 2012;117(D10):D10307.
[56] Wunch D, Wennberg PO, Toon GC, Connor BJ, Fisher B, Osterman GB, et al. A method for evaluating bias in global measurements of CO_2 total columns from space. Atmos Chem Phys 2011;11(23):12317–37.
[57] Basu S, Houweling S, Peters W, Sweeney C, Machida T, Maksyutov S, et al. The seasonal cycle amplitude of total column CO_2: factors behind the model observation mismatch. J Geophys Res 2011;116(D23):D10307.
[58] Houweling S, Aben I, Breon FM, Chevallier F, Deutscher N, Engelen R, et al. The importance of transport model uncertainties for the estimation of CO_2 sources and sinks using satellite measurements. Atmos Chem Phys 2010;10 (20):9981–92.
[59] Keppel-Aleks G, Randerson JT, Lindsay K, Stephens BB, Keith Moore J, Doney SC, et al. Atmospheric carbon dioxide variability in the community earth system model: evaluation and transient dynamics during the twentieth and twenty-first centuries. J Clim 2013;26(13):4447–75.
[60] Mu M, Randerson JT, van der Werf GR, Giglio L, Kasibhatla P, Morton D, et al. Daily and 3 hourly variability in global fire emissions and consequences for atmospheric model predictions of carbon monoxide. J Geophys Res 2011;116 (D24):D24303.
[61] Messerschmidt J, Parazoo N, Wunch D, Deutscher NM, Roehl C, Warneke T, et al. Evaluation of seasonal atmosphere–biosphere exchange estimations with TCCON measurements. Atmos Chem Phys 2013;13(10):5103–15.
[62] Wang W, Tian Y, Liu C, Sun Y, Liu W, Xie P, et al. Investigating the performance of a greenhouse gas observatory in Hefei, China. Atmos Meas Tech 2017;10 (7):2627–43.
[63] Tian Y, Sun Y, Liu C, Wang W, Shan C, Xu X, et al. Characterisation of methane variability and trends from near-infrared solar spectra over Hefei, China. Atmos Environ 2018;173:198–209.
[64] Liu HY, Jacob DJ, Bey I, Yantosca RM, Duncan BN, Sachse GW. Transport pathways for Asian pollution outflow over the Pacific: interannual and seasonal variations. J Geophys Res Atmos 2003;108(D20):8786.
[65] Geibel MC, Gerbig C, Feist DG. A new fully automated FTIR system for total column measurements of greenhouse gases. Atmos Meas Tech 2010;3 (5):1363–75.
[66] Sun Y, Liu C, Chan K, Wang W, Shan C, Hu Q, et al. The influence of instrumental line shape degradation on the partial columns of O_3, CO, CH_4 and N_2O derived from high-resolution FTIR spectrometry. Remote Sens 2018;10 (12):2041.
[67] Yin H, Sun YW, Liu C, Wang W, Shan C, Zha L, et al. Remote sensing of atmospheric hydrogen fluoride (HF) over Hefei, China with ground-based high-resolution Fourier transform infrared (FTIR) spectrometry. Remote Sens 2021;13(4):791.
[68] Rodgers CD. Inverse methods for atmospheric sounding-theory and practice. Singapore: World Scientific Publishing Co., Pte, Ltd.; 2000.
[69] Dammers E, Vigouroux C, Palm M, Mahieu E, Warneke T, Smale D, et al. Retrieval of ammonia from ground-based FTIR solar spectra. Atmos Chem Phys 2015;15(22):12789–803.
[70] Vigouroux C, Bauer Aquino CA, Bauwens M, Becker C, Blumenstock T, De Mazière M, et al. NDACC harmonized formaldehyde time series from 21 FTIR stations covering a wide range of column abundances. Atmos Meas Tech 2018;11(9):5049–73.
[71] Yin H, Sun Y, Liu C, Zhang L, Lu X, Wang W, et al. FTIR time series of stratospheric NO_2 over Hefei, China, and comparisons with OMI and GEOS-Chem model data. Opt Express 2019;27(16):A1225–40.
[72] Hase F. Improved instrumental line shape monitoring for the ground-based, high-resolution FTIR spectrometers of the network for the detection of atmospheric composition change. Atmos Meas Tech 2012;5 (3):603–10.
[73] Sun Y, Palm M, Liu C, Hase F, Griffith D, Weinzierl C, et al. The influence of instrumental line shape degradation on NDACC gas retrievals: total column and profile. Atmos Meas Tech 2018;11(5):2879–96.
[74] Pougatchev NS, Connor BJ, Rinsland CP. Infrared measurements of the ozone vertical-distribution above Kitt Peak. J Geophys Res Atmos 1995;100 (D8):16689–97.

[75] Sun Y, Palm M, Weinzierl C, Petri C, Notholt J, Wang Y, et al. Technical note: sensitivity of instrumental line shape monitoring for the ground-based high-resolution FTIR spectrometer with respect to different optical attenuators. Atmos Meas Tech 2017;10(3):989–97.
[76] Shan C, Wang W, Liu C, Sun Y, Hu Q, Xu X, et al. Regional CO emission estimated from ground-based remote sensing at Hefei site, China. Atmos Res 2019;222:25–35.
[77] Hedelius JK, He TL, Jones DBA, Baier BC, Buchholz RR, De Mazière M, et al. Evaluation of MOPITT Version 7 joint TIR–NIR X_{CO} retrievals with TCCON. Atmos Meas Tech 2019;12(10):5547–72.
[78] Yin H, Sun Y, Liu C, Lu X, Smale D, Blumenstock T, et al. Ground-based FTIR observation of hydrogen chloride (HCl) over Hefei, China, and comparisons with GEOS-Chem model data and other ground-based FTIR stations data. Opt Express 2020;28(6):8041–55.
[79] Oshio H, Yoshida Y, Matsunaga T, Deutscher NM, Dubey M, Griffith DWT, et al. Bias correction of the ratio of total column CH_4 to CO_2 retrieved from GOSAT spectra. Remote Sens 2020;12(19):3155.
[80] Shan C, Wang W, Liu C, Guo Y, Xie Y, Sun Y, et al. Retrieval of vertical profiles and tropospheric CO_2 columns based on high-resolution FTIR over Hefei. China. Opt Express 2021;29(4):4958–77.
[81] Shan C, Zhang H, Wang W, Liu C, Xie Y, Hu Q, et al. Retrieval of stratospheric HNO_3 and HCl based on ground-based high-resolution Fourier transform spectroscopy. Remote Sens 2021;13(11):2159.
[82] Vigouroux C, Blumenstock T, Coffey M, Errera Q, García O, Jones NB, et al. Trends of ozone total columns and vertical distribution from FTIR observations at eight NDACC stations around the globe. Atmos Chem Phys 2015;15(6):2915–33.
[83] Yoshida Y, Kikuchi N, Morino I, Uchino O, Oshchepkov S, Bril A, et al. Improvement of the retrieval algorithm for GOSAT SWIR X_{CO_2} and X_{CH_4} and their validation using TCCON data. Atmos Meas Tech 2013;6(6):1533–47.
[84] Rodgers CD, Connor BJ. Intercomparison of remote sounding instruments. J Geophys Res Atmos 2003;108(D3):4116.
[85] Gisi M, Hase F, Dohe S, Blumenstock T, Simon A, Keens A. X_{CO_2}-measurements with a tabletop FTS using solar absorption spectroscopy. Atmos Meas Tech 2012;5(11):2969–80.